Article

A Highly Resolved Speleothem δ^{13}C Record from Central China and Its Manifestation on Multiple Time Scales during the Last Glacial

Qingmin Chen [1,*,†], Xing Cheng [1,2,*,†] (ID), Li Deng [1,†], Kaikai He [1], Wenshuo Zhang [1], Gang Xue [2,3], Zeke Zhang [2], Le Ma [2], Gaohong Wang [1], Hai Cheng [4,5] and R. Lawrence Edwards [5]

[1] Shaanxi Experimental Center of Geological Survey, Shaanxi Institute of Geological Survey, Xi'an 710065, China
[2] State Key Laboratory of Loess and Quaternary Geology, Institute of Earth Environment, Chinese Academy of Sciences, Xi'an 710061, China
[3] State Key Laboratory of Continental Dynamics, Department of Geology, Northwest University, Xi'an 710069, China
[4] Institute of Global Environmental Change, Xi'an Jiaotong University, Xi'an 710049, China
[5] Department of Earth Sciences, University of Minnesota, Minneapolis, MN 55455, USA
*   Correspondence: chenqingmin0601@163.com (Q.C.); xingcheng529@outlook.com (X.C.)
†   These authors contribute equally to this work.

Abstract: Speleothem δ^{13}C in monsoonal China differs from speleothem δ^{18}O, which is widely used as a climatic proxy for several complex control reasons. Nevertheless, δ^{13}C records have the potential to reveal the implications of hydroclimatic changes. This study reports a speleothem δ^{13}C record from Didonghe (DDH) Cave in central China spanning 34 to 13 kyr BP. After we investigated the factors that influence speleothem δ^{13}C, we found that the δ^{13}C record showed that DDH Cave can prompt directional shifts via local hydroclimatic changes, such as in vegetation types, biomass, and rock–water interaction processes, suggesting that δ^{13}C is mainly controlled by the local hydroclimate. Ensemble empirical mode decomposition (EEMD) results revealed a coupling relationship between δ^{18}O and δ^{13}C on multiple timescales, which suggested that changes in precipitation caused by large-scale monsoonal circulation are controlled by regional hydrological conditions to a great extent. However, the hydrological conditions of the cave were relatively mild and humid during the last glacial maximum (LGM), which revealed the impact of evaporation on changes in the region's hydrological conditions. We also found that the δ^{18}O and δ^{13}C profiles decoupled when δ^{13}C changed with a shift in the location of the westerly during HS1. The δ^{13}C record correlates well with other paleoclimate records, suggesting that regional hydrological conditions are also modulated by the Earth's internal and external driving factors.

Keywords: speleothem δ^{13}C; last glacial; East Asian summer monsoon; hydroclimate

1. Introduction

Hydroclimate conditions are vital to ecosystem variations in the Qinba Mountains, which are located in an important water source area [1]. Changes in regional precipitation and hydrological conditions have significant effects on the flood disasters in the Qinba Mountains and potentially influenced ancient human settlements. Therefore, clarifying hydroclimatic changes in the Qinba Mountains is of great significance for water-using strategies. Particularly, identifying hydroclimate variations before the Anthropocene is the key to understanding the driving forces behind it. However, since this region (the Qinba area, located in central China) is subject to the Indian Monsoon (IM) and the East Asian Monsoon (EAM), its complexity has led to a poor state of research regarding the dynamic evolution of the long sequences of hydrological conditions [2].

Speleothems are one of the most important types of archives in reconstructing paleoclimate change because of their high resolution, wide distribution, and accurate dating [3–5].

Based on accurate U-series-dated chronology, a few studies have reconstructed regional hydroclimate changes using variable speleothem proxies. A previous study proposed that the difference in oxygen isotopes between two stalagmites can reflect local precipitation [6]. Later, the relative fluctuation of the local hydrology was reconstructed based on the ratio of speleothem anhysteretic remanent magnetism (ARM) to saturation isothermal remanent magnetism (SIRM) [7]. Recently, stalagmite $\delta^{13}C$ has been proposed as a potential way to reconstruct local ecological environments and hydrological climates [8,9].

Generally, speleothem $\delta^{13}C$ is controlled by vegetation and soil processes in overlying systems, percolating characteristics in seepage systems, and some cave factors [10,11]. Speleothem carbon can originate from atmospheric CO_2, biogenic CO_2 from autotrophic and heterotrophic soil respiration, and carbonate bedrock [12]. Recently, deep underground reservoirs of carbon [13] and deeply rooted vegetation [14] were recognized as crucial influence factors in the karst carbon cycle. The relative contribution degree of these different sources to stalagmite $\delta^{13}C$ is modulated by the hydroclimate and temperature. Nevertheless, by comparing other proxies, including speleothem $\delta^{18}O$, an increasing number of studies have shown that hydroclimate conditions are significant in speleothem $\delta^{13}C$ changes. For example, Novello et al. [15] determined the relationship between local hydroclimate and atmospheric convective processes related to the South American Monsoon System through a comparative study of speleothems $\delta^{13}C$ and $\delta^{18}O$. With further studies of speleothem $\delta^{13}C$, more research has suggested that $\delta^{13}C$ records can be employed to reflect hydroclimate variation by excluding the isotope kinetic fractionation process [16–21].

In some cases, stalagmite $\delta^{13}C$ may respond to millennial climate changes more sensitively than stalagmite $\delta^{18}O$. The oxygen and carbon isotope records of stalagmites in China show millennial-time-scale oscillations, for instance, some records from Hulu Cave [20,22]. Other records from stalagmites in southern China show that the amplitude of millennial-time-scale events recorded by $\delta^{13}C$ is twice as large as that of the $\delta^{18}O$ record during the last two glacial cycles [22,23]. The structural characteristics of D-O (Dansgaard–Oeschger) events documented in stalagmite $\delta^{13}C$ are more similar to the record of the NGRIP (North GRIP) ice core than the $\delta^{18}O$ stalagmite record [18,24].

This study presents a highly resolved speleothem $\delta^{13}C$ record spanning the period 34 to 13 kyr BP from Didonghe (DDH) Cave in Shaanxi Province, exploring the variations in stalagmite $\delta^{13}C$ and their implications for the local hydroclimate and related driving mechanisms.

2. Cave Setting and Study Sample

Didonghe (DDH) Cave (32°44′14″ N, 106°24′26″ E, 1262 m a.s.l.) is located in Ningqiang County, Shaanxi Province, China (Figure 1). This cave developed in the Permian Wujiaping strata with a length of 1200 m and a maximum depth of 340 m [25]. The overlying section is covered by yellow-brown soil, and the vegetation is mainly composed of evergreens, a deciduous broad-leaf mixed forest belt (Quercus, Acer), and erect shrubs (Indigofera pseudotinctoria Matsum, Lespedeza). Our previous work [25] showed that the hydrology of this cave site is mainly controlled by the ISM (Indian Summer Monsoon) and the EASM (East Asian Summer Monsoon) (Figure 1a). Data from 1957 to 2007 taken from Ningqiang Meteorological Station (Figure 1c) indicate that the mean annual temperature and the mean annual rainfall are 13 °C and 1104 mm, respectively, and the precipitation mainly falls during the summer season (from May to August) [25]. Stalagmite DDH-B15 was collected from the Yulong chamber at the deepest part of Cave B in the DDH Cave system, 2 km from the cave entrance. The length of DDH-B15 is 158 mm, and the diameter varies between 64 mm and 30 mm. After cutting a stalagmite with a diamond wire saw, the center of the stalagmite was observed to be yellowish-brown, and the two sides were yellowish-white, with some cracks. Other detailed information about the cave setting and sample description can be found in Chen and Cheng et al. [25].
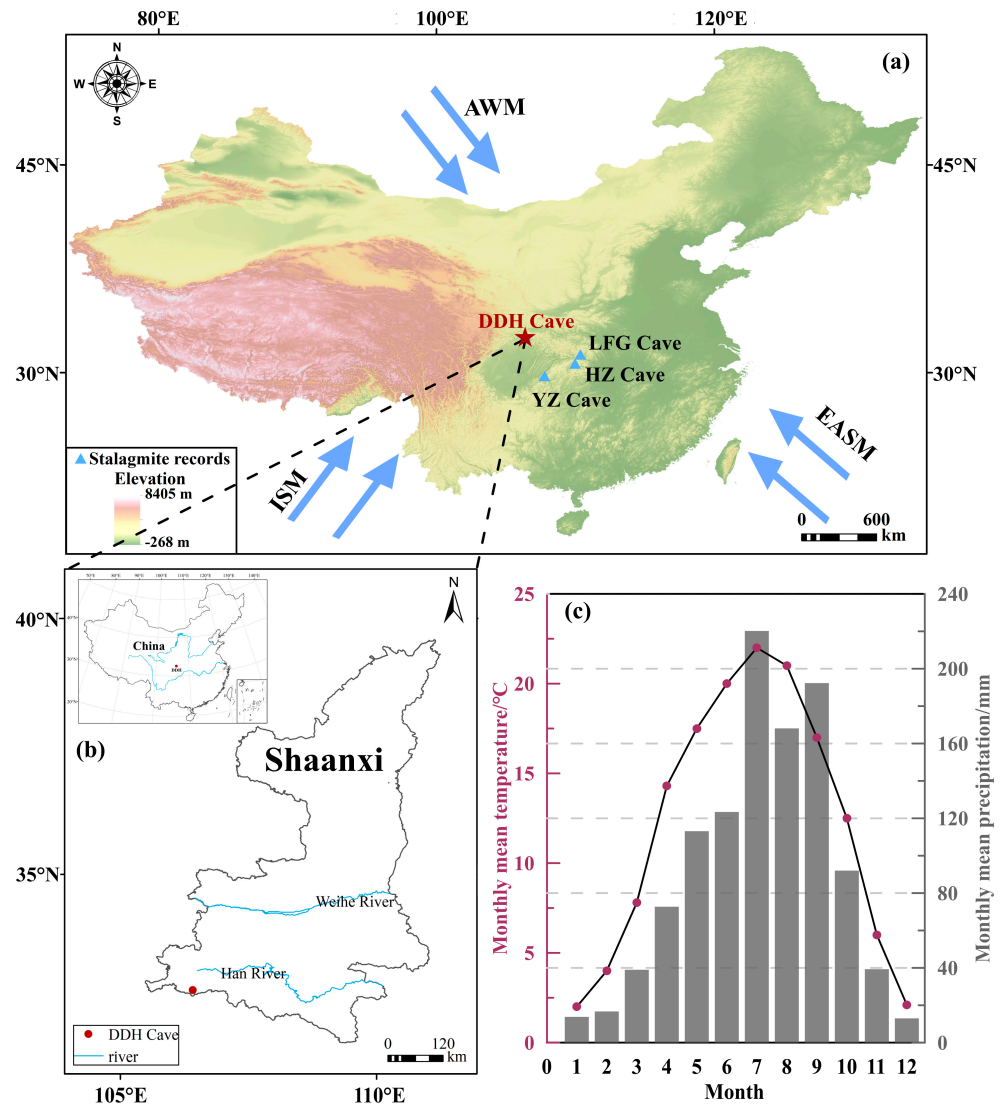
Figure 1. (**a**) Overview of the research area: the red star is DDH Cave, and the blue triangles are the other caves. (**b**) Location of Didonghe Cave. (**c**) Annual mean precipitation and temperature of Ningqiang County from 1957 to 2007 [26].

3. Methods

DDH-B15 was cut along the growth axis using a diamond wire saw and polished, and a total of 322 subsamples were drilled along the axis for stable isotope analysis at 0.5 mm intervals using a dental drill. Stable isotope analysis was performed at the Institute of Earth Environment, Chinese Academy of Sciences, using an Isoprime100 gas source stable isotope ratio mass spectrometer equipped with a MultiPrep system. To monitor the stability, laboratory internal standard samples, TB1, were measured for every 10–20 subsamples. The $\delta^{13}C$ and $\delta^{18}O$ results are relative to the Vienna Pee Dee Belemnite (VPDB) standard. We have analyzed the variability of oxygen isotopes in detail before [25]; this paper focuses on analyzing carbon isotopes.

Based on the results of a previous study [25], we drilled another 7 samples from DDH-B15 for a more accurate chronological scale and performed U-Th dating using a multi-collection inductively coupled plasma mass spectrometer (MC-ICP-MS) at the Isotope Laboratory of Xi'an Jiaotong University. The chemical procedures used to separate the uranium and thorium for ^{230}Th dating are similar to those described in Edwards et al. (1987) [27], and the measuring protocol is the same as the one used by Cheng et al.

(2013) [28]. A ^{230}Th/^{232}Th atomic ratio of $4.4 \pm 2.2 \times 10^{-6}$ was used to correct for the initial ^{230}Th.

4. Results

4.1. Age Model and Growth Rate

By combining our newly obtained dating results (Table 1) with previous U-Th dating ages [25], a new age model of DDH-B15 was established (Figure 2). The growth period of DDH-B15 spans 33.97 to 13.12 kyr BP, and the growth rate ranges from 2.3 to 14.6 mm/kyr, with a mean growth rate of 8.03 mm/kyr. Overall, the growth rate of DDH-B15 was relatively high during 34~29 kyr BP and 22~16 kyr BP, but it was low during 29~16 kyr BP.
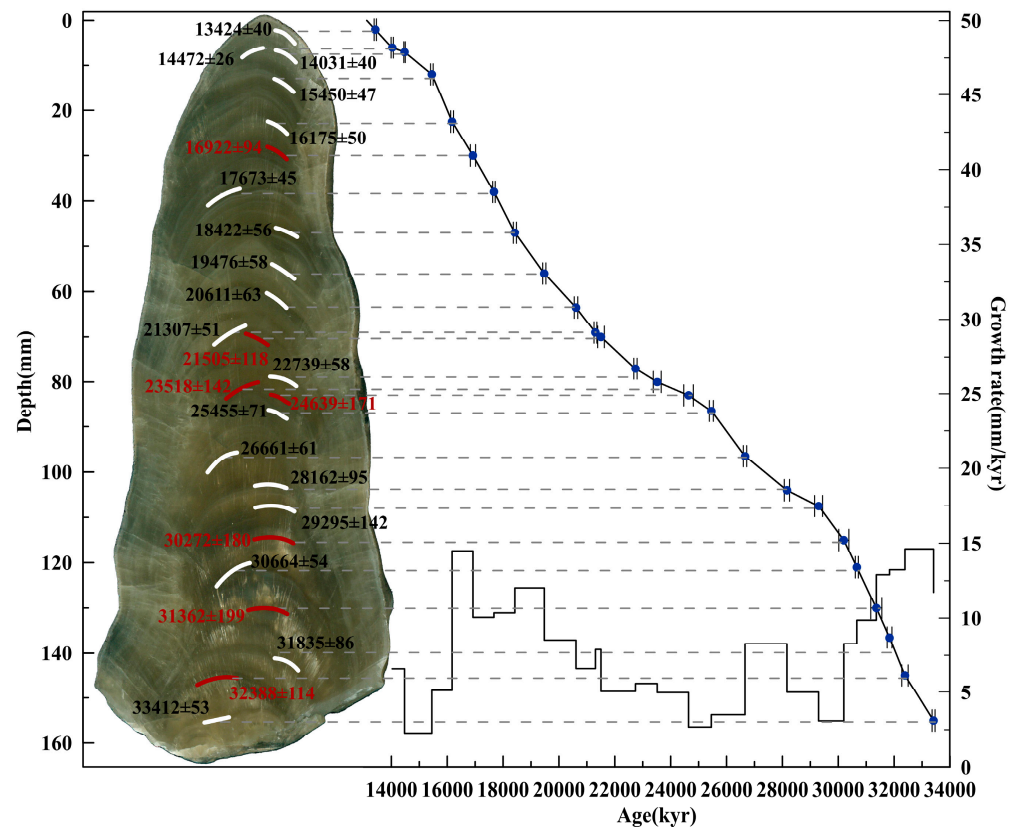
Figure 2. DDH-B15 stalagmite and age model (the white and red bars are the previous sampling positions and newly taken sampling positions, respectively).

4.2. The $\delta^{13}C$ and $\delta^{18}O$ Records

A total of 322 sets of $\delta^{13}C$ and $\delta^{18}O$ data were obtained from stalagmite DDH-B15, with an average resolution of ~64.8 years. The $\delta^{18}O$ record varies between -5.60‰ and -11.00‰, with a mean value of -8.29‰ [25] (Figure 3a). The $\delta^{13}C$ ranges from -1.16‰ to -7.73‰, with a mean value of -3.801‰, and its oscillation (6.57‰) exhibits a larger amplitude compared with $\delta^{18}O$. In accordance with oscillation amplitude, the $\delta^{13}C$ record is divided into three parts. During 34.0~26.0 kyr BP, the amplitude of $\delta^{13}C$ is relatively large, with a negative carbon isotope mean. Subsequently, the DDH-B15 $\delta^{13}C$ values gradually decrease and then oscillate around -3.08‰ until 15.0 kyr BP. After that, speleothem $\delta^{13}C$ is interrupted by a positive excursion from 15.0 to 13.12 kyr BP and followed by a decreasing trend.
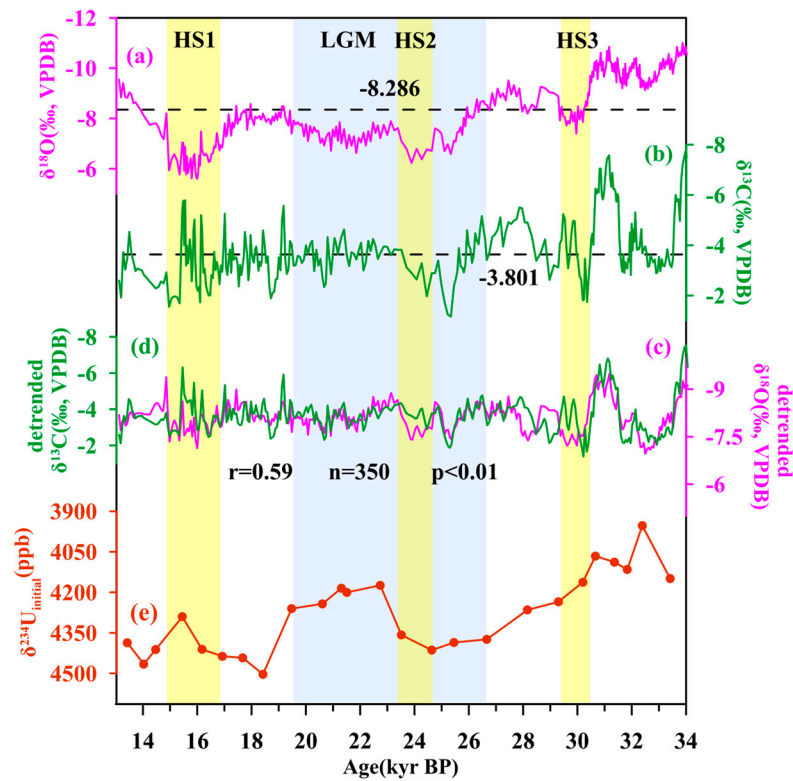
Figure 3. Time series of (**a**) original DDH δ^{18}O record; (**b**) original DDH δ^{13}C record; (**c**,**d**) detrended record of δ^{18}O and δ^{13}C; (**e**) δ^{234}U$_{initial}$. The three yellow bars are HS1, HS2, and HS3 cold events, and the blue area is the LGM period.

4.3. ^{238}U, δ^{234}U$_{initial}$, and ^{232}Th

The values of ^{238}U, δ^{234}U$_{initial}$, and ^{232}Th were acquired using a table of ^{230}Th dating results derived from DDH-B15. The value of ^{238}U ranges from 757.4 to 1245.8 ppb, with a mean value of 1007.8 ppb, while ^{232}Th fluctuates greatly and varies between 3917 ppt and 68 ppt. Most ^{232}Th values are less than 1000 ppt, except for samples collected from 2 mm and 7 mm, reflecting that most samples are barely contaminated. The δ^{234}Uinitial data show a pattern similar to the δ^{13}C record. Generally, δ^{234}U$_{initial}$ increases slightly over the period from 13.12 kyr BP to 19 kyr BP, with a significant decrease from 14.72 kyr BP to 16.17 kyr BP. This is followed by a rapid decrease to a steady low value at 22.81 kyr BP and a subsequent rise during 16.18~26.67 kyr BP. Then, δ^{234}U$_{initial}$ maintains a downward trend until 33.41 kyr BP.

Table 1. ^{230}Th supplemental dating results for DDH-B15.

Sample Number	Depth mm	^{238}U (ppb)		^{232}Th (ppt)		^{230}Th/^{232}Th (Atomic $\times 10^{-6}$)		δ^{234}U * (Measured)		^{230}Th/^{238}U (Activity)		^{230}Th Age (yr) (Uncorrected)		^{230}Th Age (yr) (Corrected)		δ^{234}U$_{initial}$ ** (Corrected)		^{230}Th Age (yr BP) *** (Corrected)	
DDH-B15	30	956.2	±3.6	516	±11	24425	±545	4436.4	±10.8	0.7999	±0.0038	16997	±94	16995	±94	4654	±11	16922	±94
DDH-B15-70	70	898.4	±3.3	157	±5	90503	±3030	4200.3	±11.9	0.9563	±0.0043	21579	±118	21578	±118	4464	±13	21505	±118
DDH-B15-80	80	990.8	±4.4	537	±12	32583	±727	4357.9	±12.4	1.0703	±0.0054	23594	±142	23591	±142	4658	±13	23518	±142
DDH-B15-83	83	985.2	±4.9	220	±7	83260	±2509	4414.1	±15.6	1.1286	±0.0064	24713	±171	24712	±171	4733	±17	24639	±171
DDH-B15-115	115	858.5	±3.5	117	±4	156823	±5552	4162.2	±12.1	1.2937	±0.0062	30273	±180	30272	±180	4533	±13	30199	±180
DDH-B15-130	130	1036.4	±4.4	139	±5	162628	±6046	4088.0	±11.2	1.3188	±0.0069	31436	±199	31435	±199	4467	±12	31362	±199
DDH-B15-145	145	875.4	±2.0	216	±6	88101	±2600	3952.9	±6.2	1.3209	±0.0038	32462	±114	32461	±114	4332	±7	32388	±114

U decay constants: $\lambda_{238} = 1.55125 \times 10^{-10}$ [29] and $\lambda_{234} = 2.82206 \times 10^{-6}$ [28]. Th decay constant: $\lambda_{230} = 9.1705 \times 10^{-6}$ [28] * δ^{234}U = ([^{234}U/^{238}U]$_{activity} - 1) \times 1000$. ** δ^{234}U$_{initial}$ was calculated based on ^{230}Th age (T), i.e., δ^{234}U$_{initial} = \delta^{234}U_{measured} \times e^{\lambda_{234} \times T}$. Corrected ^{230}Th ages assume an initial ^{230}Th/^{232}Th atomic ratio of $4.4 \pm 2.2 \times 10^{-6}$. These are the values for a material at secular equilibrium, with a bulk earth ^{232}Th/^{238}U value of 3.8. The errors are arbitrarily assumed to be 50%. *** B.P. stands for "before present", where the "present" is defined as the year A.D. 1950.

5. Discussion

5.1. Interpretation of Stalagmite $\delta^{13}C$ at DDH Cave

The Hendy test is an important way to verify whether a speleothem has formed under an isotopic equilibrium condition. If so, there should be no correlation between $\delta^{13}C$ and $\delta^{18}O$ from the same layer [30]. However, speleothems $\delta^{13}C$ and $\delta^{18}O$ can also change in the same direction if they are controlled by the same driving forces. Carbon in stalagmites mainly originates from soil CO_2 controlled by an overlying system involving soil CO_2 and organic matter degradation (80%–95%), parent rock (10%–15%), and atmospheric CO_2 (the concentration is only about 0.03%) [17,31]. Therefore, speleothem $\delta^{13}C$ is affected by the carbon source and can largely record information on vegetation variations. Nevertheless, during the percolating process, the dynamic processes in the seepage system should also be considered. Thus, we argue that the "Hendy test" cannot determine whether a dynamic fractionation exists because these factors are more or less influenced by climate.

The $\delta^{13}C$ value of C3 plants is more negative than that of C4 plants since C3 plants mainly incorporate carbon using the C3 Calvin pathway [32,33], although previous work has suggested that the relative abundance of the C3/C4 types has the greatest impact on stalagmite $\delta^{13}C$ [30]. The values of $\delta^{13}C$ under the control of C3 vegetation are more negative ($-14‰\sim-6‰$) than when they are under the control of C4 vegetation ($-6‰\sim-2‰$) [33]. Spore pollen reconstruction results have shown that ancient vegetation in central China was dominated by mixed broadleaf evergreen and deciduous forests during the last glacial maximum [34], and this kind of forest is mainly composed of C3 plants. DDH-B15 $\delta^{13}C$ ranges from $-1.16‰$ to $-7.73‰$, with a mean value of $-3.80‰$, which is largely consistent with the speleothem $\delta^{13}C$ range expected at a site overlain with C4 vegetation (-6 to $-2‰$), contradicting the spore pollen reconstruction results. Hence, the change in DDH-B15 $\delta^{13}C$ does not support the explanation of C3/C4-type vegetation changes. The densities of vegetative cover and biomass are the main controlling factors for $\delta^{13}C$ in regions dominated by C3-type vegetation [35]. As kinetic fractionation in biological processes favors ^{12}C, organically derived CO_2 is released into the soil through root respiration, and the microbial decomposition of organic matter is relatively depleted in ^{13}C [21].

Cave system conditions can also govern speleothem $\delta^{13}C$. Soil CO_2 makes a more significant contribution to speleothem carbon under an open system with relatively negative $\delta^{13}C$, and vice versa [36]. However, studies have shown that variations in the open/closed ratio are often small between speleothems from the same cave [19,37–39].

Furthermore, seasonal temperature changes can alter air pCO_2 and, hence, result in a variable gas pressure gradient between the inside and outside of a cave [21]. A higher pCO_2 gradient likely causes higher $\delta^{13}C$ values in drip water because of degassing enhancement [40,41]. The DDH-B15 $\delta^{13}C$ we collected came from deep in the cave, where the environment is relatively stable, which may show that the effect of ventilation on $\delta^{13}C$ is relatively small.

An increasing number of studies show that the regional hydroclimate is very important to variations in speleothem $\delta^{13}C$; that is, an increase in precipitation may lead to a decrease in the residence time of seepage water in epikarst, hence resulting in a lower stalagmite $\delta^{13}C$ value due to weakened bedrock dissolution and degassing [42,43].

Given the above, vegetation changes, cave system conditions, and kinetic fractionation in caves can be ruled out as the dominant influencing factors. The regional hydroclimate is likely the main driver, and although it is difficult to pinpoint one or more factors that affect speleothem $\delta^{13}C$, we can be sure that they affect it in the same direction [21,44].

5.2. The Phase Relationship between DDH-B15 $\delta^{13}C$ and $\delta^{18}O$ on Multiple Timescales

The phase relationship between speleothem $\delta^{18}O$ and $\delta^{13}C$ is still an open question. To clarify the coupling relationship between $\delta^{18}O$ and $\delta^{13}C$, we used the EEMD method to decompose DDH-B15 $\delta^{13}C$ and $\delta^{18}O$ records [45] and obtained seven intrinsic mode functions (imfs) and one residual function (res), respectively. These intrinsic mode functions were reconstructed as three signals according to different timescales (Figure 4).

On the centennial time scale, our decomposed data derived from the EEMD method showed that the major periods of DDH-B15 δ^{13}C (0.22 kyr, 0.41 kyr, and 0.87 kyr) are consistent with those of δ^{18}O (0.19 kyr, 0.37 kyr, 0.81 kyr). A correlation analysis showed a positive correlation, and the correlation coefficient between the imf1 + imf2 + imf3 values of δ^{13}C and δ^{18}O is 0.59 (*p* < 0.01). A stalagmite from Yunnan province showed that changes in temperature and precipitation due to monsoon circulation lead δ^{13}C and δ^{18}O to change in the same direction on a centennial scale [46]. A similar change mode has also been demonstrated in stalagmites in Europe, North America, and Arabia [47–49]. δ^{13}C and δ^{18}O consistencies may be attributable to hydroclimatic changes. This is because EASM dominates precipitation at our study site; it further influences the regional hydroclimate and, hence, has the same rhythm [32,50–52].

On the millennial time scale, the decomposed δ^{13}C results significantly correlated with the δ^{18}O results, with a high correlation coefficient (r = 0.53, *p* < 0.01). The covariations of speleothems δ^{13}C and δ^{18}O on the millennial scale have been confirmed with stalagmite records from southern China [21,23,53]. This strong coupling relationship may be due to a spate of weak monsoons, resulting in periodic changes in the intensity of Asian monsoon rainfall and ultimately causing variations in cave seepage water flow. Millennial-scale climatic changes, perhaps induced by Henrich events, led to a cold climate in the high latitude of the Northern Hemisphere and changed the intensity of low-latitude monsoons [54].
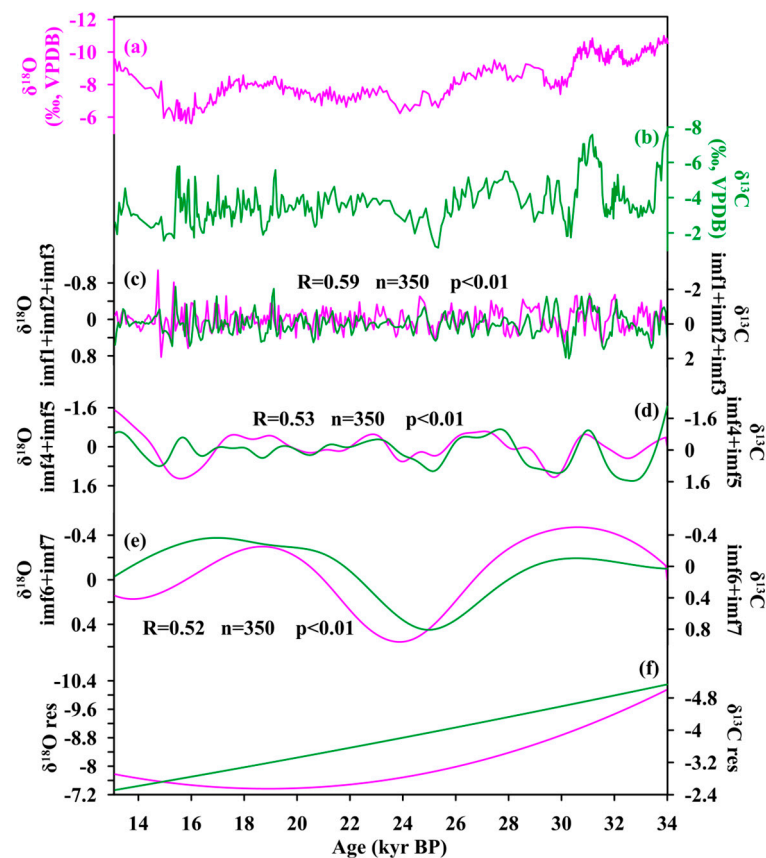
Figure 4. (**a**,**b**) Speleothems δ^{18}O (pink) and δ^{13}C (green) in DDH Cave; (**c**) imf 1–3 components of speleothems δ^{18}O and δ^{13}C; (**d**) imf 4 + 5 components of speleothems δ^{18}O and δ^{13}C; (**e**) imf 6 + 7 components of speleothems δ^{18}O and δ^{13}C; (**f**) res components of speleothems δ^{18}O and δ^{13}C.

Significantly, the HS3 and HS2 events recorded in δ^{18}O almost match the δ^{13}C record (Figure 4). However, the δ^{13}C record does not exhibit a positive trend during 16~15 kyr BP and shows an opposite structure to the δ^{18}O record (Figure 4b); in other words, the hydroclimate in DDH Cave was wet (or at least not dry) during this period. Similar phenomena appear in other stalagmite records in central China (Figure 5d,e) [55,56]. By

studying trace elements, Zhang et al. [57] found that central China experienced a humid hydrological climate (Figure 5b). The decoupling of $\delta^{13}C$ and $\delta^{18}O$ over this period may be attributable to the anticorrelation between the intensity of monsoons and the precipitation of central China may be linked to the movement of the westerly [57]. A weak AMOC (Figure 5d) led to the westerly's delayed northward migration, resulting in a prolonged Meiyu stage in central China. However, this weak AMOC in 27~25 kyr BP did not cause a moist climate in the research area. In considering this phenomenon, we assumed that its responses to climate change vary during different climate boundary conditions, especially during different HS events. The transition period from MIS3 to MIS2, a period with a decrease in summer solar insolation in the North Hemisphere [58], presents significant climatic instability.
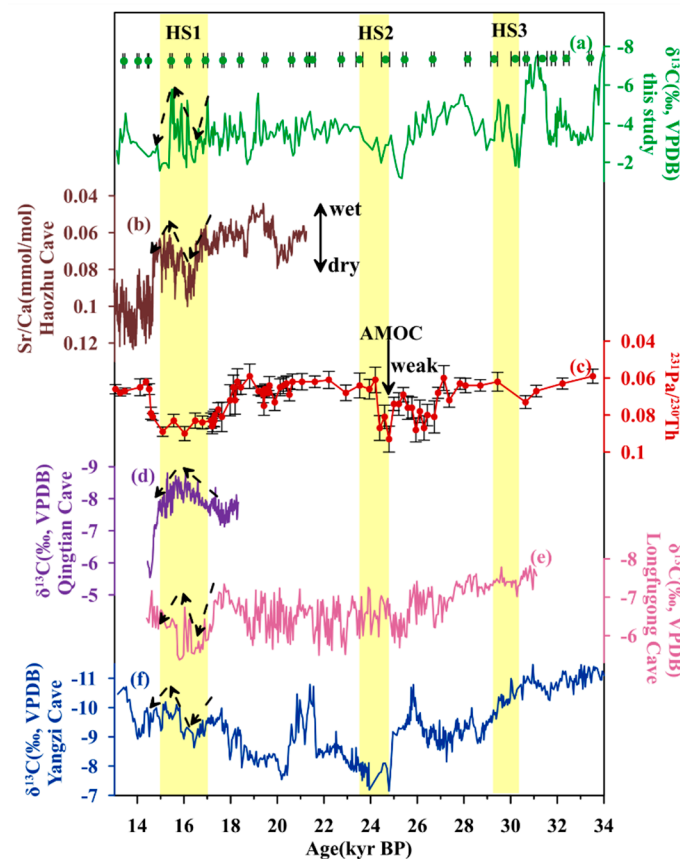
Figure 5. Comparison of DDH record (this study) to other stalagmite records: (**a**) original DDH $\delta^{13}C$ record; (**b**) stalagmite Sr/Ca in Haozhu Cave, Hubei Province [56]; (**c**) $^{231}Pa/^{230}Th$ record of the Atlantic core [59,60]; (**d**) Qingtian Cave $\delta^{13}C$ record, Hubei Province [56]; (**e**) Longfugong Cave $\delta^{13}C$ record, Hubei Province [61]; (**f**) Yangzi Cave $\delta^{13}C$ record, Chongqing City [55].

On the orbital time scale, the variance in $\delta^{18}O$ and $\delta^{13}C$ records is dominated by processional and half-precessional cycles (10.5 kyr; 21 kyr), but these two cycles are not statistically significant because the DDH Cave record is only 20,500 years long. Generally, the cycles represented by the DDH Cave $\delta^{13}C$ record's imfs are consistent with a millennial-to-centennial scale, and this relationship has important implications for the environmental significance of $\delta^{13}C$ stalagmite. The refs of stalagmite $\delta^{13}C$ and $\delta^{18}O$ on a centennial scale have cycles (0.22 kyr; 0.19 kyr) similar to the Suess cycle [62], implying the $\delta^{13}C$ and $\delta^{18}O$ stalagmites may be affected by solar activity on a centennial scale. However, the amplitude of $\delta^{13}C$ is almost twice that of $\delta^{18}O$, suggesting that $\delta^{13}C$ variance may be amplified by hydrological signals and more sensitive to climate change. On a millennial scale, the $\delta^{18}O$ and $\delta^{13}C$ records both have a 2.1 kyr cycle, which reflects climate change at high latitudes in the Northern Hemisphere. Aside from the 2.1 kyr cycle, a corresponding 5.2 kyr cycle

due to oxygen isotopes might result from a one-quarter resonance oscillation with respect to precession. The correlation coefficient between $\delta^{13}C$ and $\delta^{18}O$ on the centennial time scale is larger than that of the millennial time scale because hydroclimatic sensitivities are different on multiple time scales.

5.3. Variation in Local Hydroclimate and Its Driving Forces

The hydroclimatic changes in DDH Cave may be roughly divided into three stages based on the above analysis of its $\delta^{13}C$ variation (Figure 6a). From 34.0 to 25.0 kyr BP, the $\delta^{13}C$ values were relatively negative, with several abrupt fluctuations, indicating more precipitation and wet climate conditions. Subsequently, $\delta^{13}C$ increased slightly and kept a relatively stable level, suggesting that precipitation decreased mildly, but the local climate condition was still relatively humid and persisted up to 15.5 kyr BP. This change is also supported by pollen records. The pollen sequence from the western part of Hubei Province suggested an evolution into dark coniferous forests dominated by Abies over the LGM period, which reflects wet climate conditions [62,63].

DDH Cave stalagmite records are comparable to speleothem records from other caves during HS1 (Figure 5), and all of these records are characterized by a period with a relative increase in humidity. Therefore, at the beginning of the HS1 event, the hydrological conditions in the region deteriorated, and the climate shifted from wet to dry. However, the hydrological conditions in the region gradually improved, and the climate was humid up until 16 kyr BP, a period that lasted for about 1 kyr. The hydrological conditions in the region deteriorated again at the end of HS1. The average $\delta^{13}C$ rose to $-2.7‰$ from 15 to 14.5 kyr BP, implying that precipitation depletion continued and the climate condition started to dry. At the end of the last glacial, the global temperature rose, the ASM strengthened, and $\delta^{13}C$ gradually decreased, indicating humid hydrological conditions.

The changes in the hydrological environment of central China are related to internal and external driving factors. The changes driven by solar activity on the millennial-to-centennial time scale have had significant impacts on the climate and environment and can lead to global climate changes via feedback from the Earth's internal systems [64–67]. The most intuitive conclusion is that changes in solar activities drive the uneven distribution of energy on the Earth's surface, resulting in increased surface temperature gradients and changes in atmospheric circulation [68].

DDH-B15 $\delta^{13}C$ is consistent with the ^{10}Be record of Greenlandic ice cores, which are regarded as proxies of solar activity (Figure 6b). Previous spectrum analysis results have also shown that solar activity and the DDH $\delta^{13}C$ record have similar cycles on a millennial time scale (Figure 6d,e). Furthermore, 330 and 310 years correspond to variable oscillation mode cycles caused by the solar convective zone. Therefore, we conclude that enhanced/attenuated solar irradiance was triggered by variations in the strength of solar activity during the glacial periods, which led to an intensified/weakened thermodynamic gradient between the Asian continent and the North Pacific and contributed to increases/decreases in monsoon-related precipitation in central China [69]. Notably, the reduction in solar irradiance may have reduced regional evaporation and thus led to a reverse hydrological evolution pattern [55,70]. Lower evaporation in the glacial period instead of decreased monsoonal-driven precipitation would have played a predominant role in regional effective moisture changes [71]. This assumption provides a plausible explanation for the humid climate conditions documented in DDH Cave and other records during the LGM period.

Internal factors driven by the Earth, including the movement of the intertropical convergence zone (ITCZ), also play a crucial role in climate change [72,73]. The southward/northward shift in the ITCZ caused by changes in solar activity leads to variations in atmospheric circulation and affects the regional hydroclimate [74,75]. During 34~13 kyr BP, the DDH $\delta^{13}C$ record positively correlated with the Cariaco Basin reflectance—which was used to reflect the southward/northward shift in the ITCZ [76]—and characterized by an enhanced $\delta^{13}C$ trend corresponding to an increased reflectance value. Thus, when the

ITCZ moves southward, the intensity of ASM decreases and leads to depleted precipitation, which is consistent with previous studies [73,77,78].
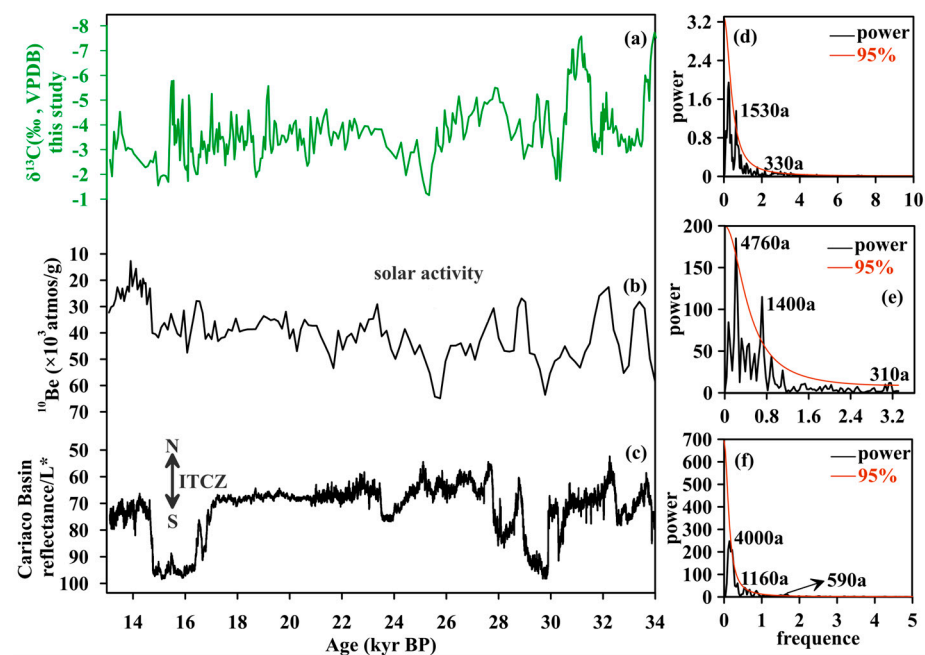
Figure 6. Comparison of the $\delta^{13}C$ stalagmite in DDH Cave with other records reflecting regional or global climate change: (**a**) $\delta^{13}C$ in this study; (**b**) ^{10}Be record of Greenlandic ice core [72]; (**c**) Cariaco Basin reflectance record [73]; (**d**) spectrum analysis of DDH $\delta^{13}C$ record; (**e**) spectrum analysis of ^{10}Be record; (**f**) spectrum analysis of Cariaco Basin reflectance record.

6. Conclusions

This study utilized highly resolved and precisely dated $\delta^{13}C$ and $\delta^{18}O$ records of the DDH-B15 stalagmite, taken from Didonghe Cave, that formed 34~13 kyr BP. We discussed the hydrological changes in central China and the relationship between carbon and oxygen isotope records. Based on the similarity between DDH-B15 $\delta^{13}C$ and other hydroclimatic indicators in the monsoonal region, we concluded that DDH-B15 $\delta^{13}C$ reflects regional hydroclimatic changes. By decomposing the data using the EEMD method, we showed that there is a coupling relationship between $\delta^{18}O$ and $\delta^{13}C$ stalagmites on multiple timescales, indicating that the Asian summer monsoon controls hydroclimatic changes in the Qinba Area. However, the $\delta^{18}O$ and $\delta^{13}C$ profiles decoupled during HS1 because the hydroclimate is susceptible to the westerly location. Our comparative analysis demonstrated that changes in regional hydrological conditions on a millennial-to-centennial scale are subject to changes caused by solar activity and superimposed by the ITCZ, which implies that the internal and external driving factors of the Earth jointly participate in regulating changes in the hydrological environment in central China in different forms.

Conflicts of Interest: The authors declare no conflicts of interest.

References

1. He, X.; Li, W.; Xu, X.; Zhao, X. Spatial-Temporal Evolution, Trade-Offs and Synergies of Ecosystem Services in the Qinba Mountains. *Sustainability* **2023**, *15*, 10352. [CrossRef]
2. Xie, S.; Hu, C.; Gu, Y.; Huang, X.; Zhu, Z.; Huang, J. Paleohydrological Variation since 13ka BP in Middle Yangtze Region. *Earth Sci.* **2015**, *40*, 198–205.
3. Yuan, D.; Cheng, H.; Edwards, R.L.; Dykoski, C.A.; Kelly, M.J.; Zhang, M.; Qing, J.; Lin, Y.; Wang, Y.; Wu, J.; et al. Timing, duration, and transitions of the last interglacial Asian monsoon. *Science* **2004**, *304*, 575–578. [CrossRef] [PubMed]
4. Cheng, H.; Ai, S.; Wang, X.; Wang, Y.; Kong, X.; Yuan, D.; Zhang, M.; Lin, Y.; Qin, J.; Ran, J. Oxygen isotope records of stalagmites from southern China. *Quat. Sci.* **2005**, *25*, 157–163.
5. Zhou, H.; Zhao, J.-x.; Feng, Y.; Chen, Q.; Mi, X.; Shen, C.-C.; He, H.; Yang, L.; Liu, S.; Chen, L.; et al. Heinrich event 4 and Dansgaard/Oeschger events 5-10 recorded by high-resolution speleothem oxygen isotope data from central China. *Quat. Res.* **2014**, *82*, 394–404. [CrossRef]
6. Hu, C.; Henderson, G.M.; Huang, J.; Xie, S.; Sun, Y.; Johnson, K.R. Quantification of Holocene Asian monsoon rainfall from spatially separated cave records. *Earth Planet. Sci. Lett.* **2008**, *266*, 221–232. [CrossRef]
7. Xie, S.C.; Evershed, R.P.; Huang, X.Y.; Zhu, Z.M.; Pancost, R.D.; Meyers, P.A.; Gong, L.F.; Hu, C.Y.; Huang, J.H.; Zhang, S.H.; et al. Concordant monsoon-driven postglacial hydrological changes in peat and stalagmite records and their impacts on prehistoric cultures in central China. *Geology* **2013**, *41*, 827–830. [CrossRef]
8. Chen, C.-J.; Huang, R.; Yuan, D.-X.; Zhang, J.; Cheng, H.; Ning, Y.-F.; Yu, T.-L.; Shen, C.-C.; Edwards, R.L.; Long, X.-Y.; et al. Karst hydrological changes during the Late-Holocene in Southwestern China. *Quat. Sci. Rev.* **2021**, *258*, 106865. [CrossRef]
9. Jia, W.; Zhang, P.; Zhang, L.; Li, X.; Gao, T.; Wang, H.; Zhang, H.; Li, H.; Cheng, H.; Edwards, R.L. Highly resolved δ^{13}C and trace element ratios of precisely dated stalagmite from northwestern China: Hydroclimate reconstruction during the last two millennia. *Quat. Sci. Rev.* **2022**, *291*, 107473. [CrossRef]
10. Tan, L.; Zhang, H.; Qin, S.; An, Z. Climatic and Anthropogenic Impacts on delta C-13 Variations in a Stalagmite from Central China. *Terr. Atmos. Ocean. Sci.* **2013**, *24*, 333–343. [CrossRef]
11. Voarintsoa, N.R.G.; Therre, S. Using the triple proxy $\delta13$C–radiocarbon–major and trace elements to understand stalagmite stable carbon composition in Madagascar. *Chem. Geol.* **2022**, *608*, 121044. [CrossRef]
12. Lechleitner, F.A.; Day, C.C.; Kost, O.; Wilhelm, M.; Haghipour, N.; Henderson, G.M.; Stoll, H.M. Stalagmite carbon isotopes suggest deglacial increase in soil respiration in western Europe driven by temperature change. *Clim. Past* **2021**, *17*, 1903–1918. [CrossRef]
13. Mattey, D.P.; Atkinson, T.C.; Barker, J.A.; Fisher, R.; Latin, J.P.; Durrell, R.; Ainsworth, M. Carbon dioxide, ground air and carbon cycling in Gibraltar karst. *Geochim. Et Cosmochim. Acta* **2016**, *184*, 88–113. [CrossRef]
14. Breecker, D.O.; Payne, A.E.; Quade, J.; Banner, J.L.; Ball, C.E.; Meyer, K.W.; Cowan, B.D. The sources and sinks of CO_2 in caves under mixed woodland and grassland vegetation. *Geochim. Et Cosmochim. Acta* **2012**, *96*, 230–246. [CrossRef]
15. Novello, V.F.; William da Cruz, F.; Vuille, M.; Pereira Silveira Campos, J.L.; Stríkis, N.M.; Apaéstegui, J.; Moquet, J.S.; Azevedo, V.; Ampuero, A.; Utida, G.; et al. Investigating δ^{13}C values in stalagmites from tropical South America for the last two millennia. *Quat. Sci. Rev.* **2021**, *255*, 106822. [CrossRef]
16. Frisia, S.; Fairchild, I.J.; Fohlmeister, J.; Miorandi, R.; Spoetl, C.; Borsato, A. Carbon mass-balance modelling and carbon isotope exchange processes in dynamic caves. *Geochim. Et Cosmochim. Acta* **2011**, *75*, 380–400. [CrossRef]
17. Genty, D.; Baker, A.; Massault, M.; Proctor, C.; Gilmour, M.; Pons-Branchu, E.; Hamelin, B. Dead carbon in stalagmites: Carbonate bedrock paleodissolution vs. ageing of soil organic matter. Implications for C-13 variations in speleothems. *Geochim. Et Cosmochim. Acta* **2001**, *65*, 3443–3457. [CrossRef]
18. Genty, D.; Blamart, D.; Ouahdi, R.; Gilmour, M.; Baker, A.; Jouzel, J.; Van-Exter, S. Precise dating of Dansgaard-Oeschger climate oscillations in western Europe from stalagmite data. *Nature* **2003**, *421*, 833–837. [CrossRef] [PubMed]
19. Riechelman, D.F.C.; Fohlmeister, J.; Kluge, T.; Jochum, K.P.; Richter, D.K.; Deininger, M.; Friedrich, R.; Frank, N.; Scholz, D. Evaluating the potential of tree-ring methodology for cross-dating of three annually laminated stalagmites from Zoolithencave (SE Germany). *Quat. Geochronol.* **2019**, *52*, 37–50. [CrossRef]
20. Liang, Y.; Wang, Y.; Wang, Q.; Wu, J.; Shao, Q.; Zhang, Z.; Yang, S.; Kong, X.; Edwards, R.L. East Asian summer monsoon climates and cave hydrological cycles over Dansgaard-Oeschger events 14 to 11 revealed by a new stalagmite record from Hulu Cave. *Quat. Res.* **2019**, *92*, 725–737. [CrossRef]

21. Cosford, J.; Qing, H.; Mattey, D.; Eglington, B.; Zhang, M. Climatic and local effects on stalagmite δ13C values at Lianhua Cave, China. *Palaeogeogr. Palaeoclimatol. Palaeoecol.* **2009**, *280*, 235–244. [CrossRef]

22. Wang, Q.; Wang, Y.; Shao, Q.; Liang, Y.; Zhang, Z.; Kong, X. Millennial-scale Asian monsoon variability during the late Marine Isotope Stage 6 from Hulu Cave, China. *Quat. Res.* **2018**, *90*, 394–405. [CrossRef]

23. Liu, D.; Wang, Y.; Cheng, H.; Edwards, R.L.; Kong, X.; Li, T.Y. Strong coupling of centennial-scale changes of Asian monsoon and soil processes derived from stalagmite δ18O and δ13C records, southern China. *Quat. Res.* **2016**, *85*, 333–346. [CrossRef]

24. Fleitmann, D. Timing and climatic expression of Dansgaard-Oeschger events in stalagmites from Sofular Cave, Turkey. *Quat. Int.* **2012**, *279–280*, 147. [CrossRef]

25. Chen, Q.; Cheng, X.; Cai, Y.; Luo, Q.; Zhang, J.; Tang, L.; Hu, Y.; Ren, J.; Wang, P.; Wang, Y.; et al. Asian Summer Monsoon Changes Inferred From a Stalagmite δ18O Record in Central China During the Last Glacial Period. *Front. Earth Sci.* **2022**, *10*, 863829. [CrossRef]

26. Hu, Y.; Lu, X.; Su, J. Analysis on Climatic Characteristics of Ningqiang County in Recent 51 Years. *J. Shaanxi Meteorol.* **2010**, *3*, 18–21.

27. Edwards, R.L.; Chen, J.H.; Wasserburg, G.J. 238U-234U-230Th-232Th systematics and the precise measurement of time over the past 500,000 years. *Earth Planet. Sci. Lett.* **1987**, *81*, 175–192. [CrossRef]

28. Cheng, H.; Edwards, R.L.; Shen, C.-C.; Polyak, V.J.; Asmerom, Y.; Woodhead, J.; Hellstrom, J.; Wang, Y.; Kong, X.; Spoetl, C.; et al. Improvements in Th-230 dating, Th-230 and U-234 half-life values, and U-Th isotopic measurements by multi-collector inductively coupled plasma mass spectrometry. *Earth Planet. Sci. Lett.* **2013**, *371*, 82–91. [CrossRef]

29. Jaffey, A.H.; Flynn, K.F.; Glendenin, L.E.; Bentley, W.C.; Essling, A.M. Precision Measurement of Half-Lives and Specific Activities of U-235 and U-238. *Phys. Rev. C* **1971**, *4*, 1889–1906. [CrossRef]

30. Hendy, C.H.J.G.E.C.A. The isotopic geochemistry of speleothems; 1, The calculation of the effects of different modes of formation on the isotopic composition of speleothems and their applicability as paleoclimatic indicators. *Geochim. Et Cosmochim. Acta* **1971**, *35*, 801–824. [CrossRef]

31. Meyer, K.W.; Feng, W.; Breecker, D.O.; Banner, J.L.; Guilfoyle, A. Interpretation of speleothem calcite δ13C variations: Evidence from monitoring soil CO_2, drip water, and modern speleothem calcite in central Texas. *Geochim. Et Cosmochim. Acta* **2014**, *142*, 281–298. [CrossRef]

32. Dorale, J.A.; Gonzalez, L.A.; Reagan, M.K.; Pickett, D.A.; Murrell, M.T.; Baker, R.G. A High-Resolution Record of Holocene Climate Change in Speleothem Calcite from Cold Water Cave, Northeast Iowa. *Science* **1992**, *258*, 1626–1630. [CrossRef] [PubMed]

33. McDermott, F. Palaeo-climate reconstruction from stable isotope variations in speleothems: A review. *Quat. Sci. Rev.* **2004**, *23*, 901–918. [CrossRef]

34. Song, M.; Dodson, J.; Lu, F.; Shi, G.; Yan, H. A continuous paleorecord of vegetation and environmental change from Erxianyan Wetland over the past 60,000 years in central China. *Palaeogeogr. Palaeoclimatol. Palaeoecol.* **2023**, *613*, 111399. [CrossRef]

35. Baldini, J.U.L.; McDermott, F.; Baker, A.; Baldini, L.M.; Mattey, D.P.; Railsback, L.B. Biomass effects on stalagmite growth and isotope ratios: A 20th century analogue from Wiltshire, England. *Earth Planet. Sci. Lett.* **2005**, *240*, 486–494. [CrossRef]

36. Fairchild, I.J.; Smith, C.L.; Baker, A.; Fuller, L.; Spotl, C.; Mattey, D.; McDermott, F. Modification and preservation of environmental signals in speleothems. *Earth-Sci. Rev.* **2006**, *75*, 105–153. [CrossRef]

37. Lechleitner, F.A.; Baldini, J.U.L.; Breitenbach, S.F.M.; Fohlmeister, J.; McIntyre, C.; Goswami, B.; Jamieson, R.A.; van der Voort, T.S.; Prufer, K.; Marwan, N.; et al. Hydrological and climatological controls on radiocarbon concentrations in a tropical stalagmite. *Geochim. Et Cosmochim. Acta* **2016**, *194*, 233–252. [CrossRef]

38. Demeny, A.; Kern, Z.; Czuppon, G.; Nemeth, A.; Leel-Ossy, S.; Siklosy, Z.; Lin, K.; Hu, H.-M.; Shen, C.-C.; Vennemann, T.W.; et al. Stable isotope compositions of speleothems from the last interglacial—Spatial patterns of climate fluctuations in Europe. *Quat. Sci. Rev.* **2017**, *161*, 68–80. [CrossRef]

39. Markowska, M.; Fohlmeister, J.; Treble, P.C.; Baker, A.; Hua, Q. Modelling the 14C bomb-pulse in young speleothems using a soil carbon continuum model. *Geochim. Et Cosmochim. Acta* **2019**, *261*, 342–367. [CrossRef]

40. Mattey, D.; Lowry, D.; Duffet, J.; Fisher, R.; Hodge, E.; Frisia, S. A 53 year seasonally resolved oxygen and carbon isotope record from a modem Gibraltar speleothem: Reconstructed drip water and relationship to local precipitation. *Earth Planet. Sci. Lett.* **2008**, *269*, 80–95. [CrossRef]

41. Spotl, C.; Fairchild, I.J.; Tooth, A.F. Cave air control on dripwater geochemistry, Obir Caves (Austria): Implications for speleothem deposition in dynamically ventilated caves. *Geochim. Et Cosmochim. Acta* **2005**, *69*, 2451–2468. [CrossRef]

42. Baker, A.; Ito, E.; Smart, P.L.; Mcewan, R.F. Elevated and variable values of 13C in speleothems in a British cave system. *Chem. Geol.* **1997**, *136*, 263–270. [CrossRef]

43. Duan, W.; Tan, M.; Ma, Z.; Cheng, H. The palaeoenvironmental significance of δ13C of stalagmite BW-1 from Beijing, China during Younger Dryas intervals inferred from the grey level profile. *Boreas* **2014**, *43*, 243–250. [CrossRef]

44. Yang, S.; Chen, S.; Wang, Y.; Shao, Q.; Tan, L.; Zhang, Z.; Zhao, K.; Wang, Z.; Liang, Y.; Zhai, X.; et al. Millennial-scale changes in the Asian monsoon during the MIS12 period as recorded by a Chinese stalagmite. *Palaeogeogr. Palaeoclimatol. Palaeoecol.* **2023**, *626*, 111698. [CrossRef]

45. Wu, Z.; Huang, N. Ensemble Empirical Mode Decomposition: A Noise-Assisted Data Analysis Method. *Adv. Adapt. Data Anal.* **2009**, *1*, 1–41. [CrossRef]

46. Zhu, X.; Zhang, M.; Cheng, H.; Wu, X.; Edwards, R.L. Centennial-scale monsoon climate fluctuations from a stalagmite record during the mid-Holocene Epoch in Fulu cave of Huaping, Yunnan, China. *Environ. Earth Sci.* **2015**, *74*, 929–935. [CrossRef]

47. Kotlia, B.S.; Singh, A.K.; Joshi, L.M.; Dhaila, B.S. Precipitation variability in the Indian Central Himalaya during last ca. 4000 years inferred from a speleothem record: Impact of Indian Summer Monsoon (ISM) and Westerlies. *Quat. Int.* **2015**, *371*, 244–253. [CrossRef]

48. Springer, G.S.; Rowe, H.D.; Hardt, B.; Edwards, R.L.; Cheng, H. Solar forcing of Holocene droughts in a stalagmite record from West Virginia in east-central North America. *Geophys. Res. Lett.* **2008**, *35*. [CrossRef]

49. Fleitmann, D.; Haldon, J.; Bradley, R.S.; Burns sj Cheng, H.; Edwards, R.L.; Raible, C.C.; Jacobson, M.; Matter, A. Droughts and societal change: The environmental context for the emergence of Islam in late Antique Arabia. *Science* **2022**, *376*, 1317–1321. [CrossRef] [PubMed]

50. Arnone, J.A., III; Verburg, P.S.J.; Johnson, D.W.; Larsen, J.D.; Jasoni, R.L.; Lucchesi, A.J.; Batts, C.M.; von Nagy, C.; Coulombe, W.G.; Schorran, D.E.; et al. Prolonged suppression of ecosystem carbon dioxide uptake after an anomalously warm year. *Nature* **2008**, *455*, 383–386. [CrossRef] [PubMed]

51. Gruenzweig, J.M.; Hemming, D.; Maseyk, K.; Lin, T.; Rotenberg, E.; Raz-Yaseef, N.; Falloon, P.D.; Yakir, D. Water limitation to soil CO_2 efflux in a pine forest at the semiarid "timberline". *J. Geophys. Res.-Biogeosciences* **2009**, *114*. [CrossRef]

52. Fohlmeister, J.; Voarintsoa, N.R.G.; Lechleitner, F.A.; Boyd, M.; Brandstaetter, S.; Jacobson, M.J.; Oster, J.L. Main controls on the stable carbon isotope composition of speleothems. *Geochim. Et Cosmochim. Acta* **2020**, *279*, 67–87. [CrossRef]

53. Zhang, J.; Liu, S.; Liu, D.; Kong, X.; Fang, Y. Correlation between oxygen and carbon isotopes of speleothems from Tian'e Cave, central China: Insights into the phase relationship between Asian summer and winter monsoons. *J. Asian Earth Sci.* **2019**, *180*, 103884. [CrossRef]

54. Porter, S.; Zhisheng, A. Correlation between Climate Events in the North-Atlantic and China during Last Glaciation. *Nature* **1995**, *375*, 305–308. [CrossRef]

55. Wu, Y.; Li, T.-Y.; Yu, T.-L.; Shen, C.-C.; Chen, C.-J.; Zhang, J.; Li, J.-Y.; Wang, T.; Huang, R.; Xiao, S.-Y. Variation of the Asian summer monsoon since the last glacial-interglacial recorded in a stalagmite from southwest China. *Quat. Sci. Rev.* **2020**, *234*, 106261. [CrossRef]

56. Zhang, W.; Wu, J.; Wang, Y.; Wang, Y.; Cheng, H.; Kong, X.; Duan, F. A detailed East Asian monsoon history surrounding the 'Mystery Interval' derived from three Chinese speleothem records. *Quat. Res.* **2017**, *82*, 154–163. [CrossRef]

57. Zhang, H.; Griffiths, M.L.; Chiang, J.C.H.; Kong, W.; Wu, S.; Atwood, A.; Huang, J.; Cheng, H.; Ning, Y.; Xie, S. East Asian hydroclimate modulated by the position of the westerlies during Termination I. *Science* **2018**, *362*, 580. [CrossRef] [PubMed]

58. Berger, A. Long-Term Variations of Daily Insolation and Quaternary Climatic Changes. *J. Atmos. Sci.* **1978**, *35*, 2362–2367. [CrossRef]

59. McManus, J.F.; Francois, R.; Gherardi, J.M.; Keigwin, L.D.; Brown-Leger, S. Collapse and rapid resumption of Atlantic meridional circulation linked to deglacial climate changes. *Nature* **2004**, *428*, 834–837. [CrossRef] [PubMed]

60. Henry, L.G.; McManus, J.F.; Curry, W.B.; Roberts, N.L.; Piotrowski, A.M.; Keigwin, L.D. North Atlantic ocean circulation and abrupt climate change during the last glaciation. *Science* **2016**, *353*, 470–474. [CrossRef] [PubMed]

61. Zhang, Z.; Wang, Y.; Yang, Z.; Liang, Y.; Yang, S.; Shao, Q.; Zhang, W.; Huang, W. Century-scale climatic oscillations during the Last Glacial Maximum revealed by stalagmite isotopic records from Longfugong Cave, China. *Environ. Earth Sci.* **2020**, *79*, 517. [CrossRef]

62. Suess, H.E. The Radiocarbon Record in Tree Rings of the Last 8000 Years. *Radiocarbon* **1980**, *22*, 200–209. [CrossRef]

63. Zhu, C.; Ma, C.M.; YUS, Y.; Tang, L.Y.; Zhang, W.Q.; Lu, X.F. A detailed pollen record of vegetation and climate changes in Central China during the past 16 000 years. *Boreas* **2010**, *39*, 69–76. [CrossRef]

64. Xiao, J.; Shang, Z.; Shu, Q.; Yin, J.; Wu, X. The vegetation feature and palaeoenvironment significance in the mountainous interior of southern China from the Last Glacial Maximum. *Sci. China Earth Sci.* **2017**, *61*, 71–81. [CrossRef]

65. Wang, Y.; Cheng, H.; Edwards, R.L.; He, Y.; Kong, X.; An, Z.; Wu, J.; Kelly, M.J.; Dykoski, C.A.; Li, X. The Holocene Asian monsoon: Links to solar changes and North Atlantic climate. *Science* **2005**, *308*, 854–857. [CrossRef] [PubMed]

66. Sha, L.; Jiang, H.; Seidenkrantz, M.-S.; Muscheler, R.; Zhang, X.; Knudsen, M.F.; Olsen, J.; Knudsen, K.L.; Zhang, W. Solar forcing as an important trigger for West Greenland sea-ice variability over the last millennium. *Quat. Sci. Rev.* **2016**, *131*, 148–156. [CrossRef]

67. Bond, G.; Kromer, B.; Beer, J.; Muscheler, R.; Evans, M.N.; Showers, W.; Hoffmann, S.; Lotti-Bond, R.; Hajdas, I.; Bonani, G. Persistent solar influence on north Atlantic climate during the Holocene. *Science* **2001**, *294*, 2130–2136. [CrossRef] [PubMed]

68. Zhao, J.; Cheng, H.; Yang, Y.; Liu, W.; Zhang, H.; Li, X.; Li, H.; Ait-Brahim, Y.; Perez-Mejias, C.; Qu, X. Role of the Summer Monsoon Variability in the Collapse of the Ming Dynasty: Evidences from Speleothem Records. *Geophys. Res. Lett.* **2021**, *48*, e2021GL093071. [CrossRef]

69. Cheng, H.; Spoetl, C.; Breitenbach, S.F.M.; Sinha, A.; Wassenburg, J.A.; Jochum, K.P.; Scholz, D.; Li, X.; Yi, L.; Peng, Y.; et al. Climate variations of Central Asia on orbital to millennial timescales. *Sci. Rep.* **2016**, *6*, 36975. [CrossRef] [PubMed]

70. Wang, Z.; Chen, S.; Wang, Y.; Zhao, K.; Liang, Y.; Li, X.; Zhang, J.; Yang, S.; Zhang, Z.; Chen, G.; et al. Climatic implication of stalagmite $\delta^{13}C$ in the middle reaches of the Yangtze River since the Last Glacial Maximum and coupling with $\delta^{18}O$. *Palaeogeogr. Palaeoclimatol. Palaeoecol.* **2022**, *608*, 111290. [CrossRef]

71. He, Y.; Zhao, C.; Zheng, Z.; Liu, Z.; Wang, N.; Li, J.; Cheddadi, R. Peatland evolution and associated environmental changes in central China over the past 40,000 years. *Quat. Res.* **2017**, *84*, 255–261. [CrossRef]
72. Finkel, R.C.; Nishiizumi, K. Beryllium 10 concentrations in the Greenland Ice Sheet Project 2 ice core from 3-40 ka. *J. Geophys. Res. Ocean.* **1997**, *102*, 26699–26706. [CrossRef]
73. Deplazes, G.; Lueckge, A.; Peterson, L.C.; Timmermann, A.; Hamann, Y.; Hughen, K.A.; Roehl, U.; Laj, C.; Cane, M.A.; Sigman, D.M.; et al. Links between tropical rainfall and North Atlantic climate during the last glacial period. *Nat. Geosci.* **2013**, *6*, 213–217. [CrossRef]
74. Emile-Geay, J.; Cane, M.; Seager, R.; Kaplan, A.; Almasi, P. El Nino as a mediator of the solar influence on climate. *Paleoceanography* **2007**, *22*. [CrossRef]
75. Duan, F.; Zhang, Z.; Wang, Y.; Chen, J.; Liao, Z.; Chen, S.; Shao, Q.; Zhao, K. Hydrological variations in central China over the past millennium and their links to the tropical Pacific and North Atlantic oceans. *Clim. Past* **2020**, *16*, 475–485. [CrossRef]
76. Chiang, J.C.H.; Bitz, C.M. Influence of high latitude ice cover on the marine Intertropical Convergence Zone. *Clim. Dyn.* **2005**, *25*, 477–496. [CrossRef]
77. Tan, L.; Shen, C.-C.; Lowemark, L.; Chawchai, S.; Edwards, R.L.; Cai, Y.; Breitenbach, S.F.M.; Cheng, H.J.; Chou, Y.-C.; Duerrast, H.; et al. Rainfall variations in central Indo-Pacific over the past 2,700 y. *Proc. Natl. Acad. Sci. USA* **2019**, *116*, 17201–17206. [CrossRef] [PubMed]
78. Zhang, H.; Cheng, H.; Spoetl, C.; Cai, Y.; Sinha, A.; Tan, L.; Yi, L.; Yan, H.; Kathayat, G.; Ning, Y.; et al. A 200-year annually laminated stalagmite record of precipitation seasonality in southeastern China and its linkages to ENSO and PDO. *Sci. Rep.* **2018**, *8*, 12344. [CrossRef] [PubMed]